Inorganic Chemistry

Article

pubs.acs.org/IC

Cis/Trans Isomerizations in Diiron Complexes Involving Aniline or Anilide Ligands

Eric Gouré,[†] Michaël Carboni,[†] Patrick Dubourdeaux,[†] Martin Clémancey,[†,‡] Ramachandran Balasubramanian,[†,§] Colette Lebrun,[⊥,∥] Pierre-Alain Bayle,[∥,¶] Pascale Maldivi,[⊥,∥] Geneviève Blondin,*[,†,§] and Jean-Marc Latour*[,†]

[†]CEA, iRTSV/LCBM, pmb, F-38000 Grenoble, France

[‡]Université Grenoble Alpes, iRTSV/LCBM, pmb, F-38000 Grenoble, France

[§]CNRS, iRTSV/LCBM, pmb, F-38000 Grenoble, France

[⊥]Université Grenoble Alpes, INAC-SCIB, RICC, F-38000 Grenoble, France

[∥]CEA, INAC-SCIB, F-38000 Grenoble, France

[¶]Université Grenoble Alpes, INAC-SCIB, RM, F-38000 Grenoble, France

Supporting Information

ABSTRACT: We have recently reported a deprotonation-induced valence inversion within a phenoxido-bridged mixed-valent diiron(II,III) complex. The initial aniline coordinated to the Fe^{II} site reacts with triethylamine, and the resulting complex contains an anilide ligand coordinated to the Fe^{III} ion. The behavior of these complexes in acetonitrile is indeed more intricate. Owing to the very distinctive spectroscopic signatures of the complexes, the conjunction of NMR, Mössbauer, and UV−visible absorption spectroscopies allows one to evidence two isomerization reactions, one involving the aniline linked to Fe^{II} and the other the anilide on Fe^{III}. Theoretical calculations sustain this conclusion. Aniline in the cis position versus the bridging phenoxide is shown to be the most stable isomer while the anilide trans to the phenoxido bridge is favored. The trans isomer of the aniline complex is more acidic than the cis one by 1 pK_a unit. Isomerization of the anilide complex is 10 times faster than the analogous isomerization of the aniline complex. Both reactions are proposed to proceed through a unique mechanism. This is the first time that such isomerization reactions are evidenced in dinuclear complexes.

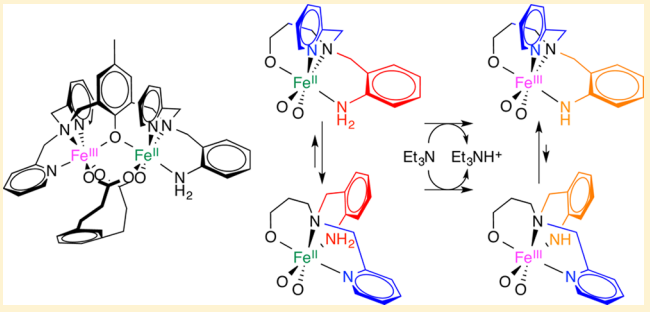

INTRODUCTION

Aniline is among the least coordinating nitrogen ligands, and only a few aniline iron complexes have been structurally characterized. Most of these complexes involve chelating anilines, with formation of the chelate assisting the binding of aniline. This view is supported by the fact that the Fe−$N_{aniline}$ distances in hexacoordinate high-spin iron(II) complexes average 2.29 Å when the aniline is unsupported[1−3] and 2.20 Å when it is chelating.[3−6] With the goal to obtain potential biomimetic models of arylamine oxygenases,[7] we prepared a diiron complex of a binucleating aniline ligand, $[Fe_2(L\text{-}BnNH_2)(mpdp)](ClO_4)_2{\cdot}H_2O$ (**1**).[8] The X-ray structure revealed that **1** possesses a triply bridged core, $[Fe^{III}(\mu\text{-}OPh)(\mu_2\text{-}mpdp)Fe^{II}(NH_2Bn)]$ ($mpdp^{2-}$ = *m*-phenylenedipropionate), and bears a terminal aminophenyl ligand in the trans position with respect to the bridging phenoxide (Scheme 1). Interestingly, we found that, upon the addition of a nitrogenous base (e.g., triethylamine), the aminophenyl ligand can be reversibly deprotonated to the anilide complex **2**, whose core $[Fe^{II}(\mu\text{-}OPh)(\mu_2\text{-}mpdp)Fe^{III}(NHBn)]$ features an inversion of the iron valences. This was the first example of a (de)-protonation-induced valence inversion for both a homodinuclear complex and first-row transition metals. A thorough electrochemical study indicated that electron transfer and proton exchange are concerted events.[9]

In order to gain more insight into the deprotonation-induced valence inversion, we investigated further the solution behavior of **1** and **2** and discovered that in an acetonitrile solution the aniline complex **1** transforms spontaneously over 2 h into another species of the same formula. Similarly, **2** transforms into another species over a shorter time scale of 20 min. This article describes an in-depth study of these transformations using Mössbauer monitoring and NMR and UV−visible kinetic studies. Indeed, both **1** and **2** possess very rich and distinctive spectroscopic properties that allow one to monitor and quantitate their transformations. These studies strongly suggest that the transformations under consideration are most probably

Received: March 4, 2014
Published: September 25, 2014

   dx.doi.org/10.1021/ic501793v | *Inorg. Chem.* 2014, 53, 10060−10069

Scheme 1. (A) Ditopic Ligand HL-BnNH$_2$ and Related Ligands and (B) Interconversion between the Forms 1t and 1c of Complex 1, on the One Hand, and 2t and 2c of Complex 2, on the Other Hand, with the Equilibrium Constant K_1 and K_2 Expressed as a Function of the Rate Constants[a]

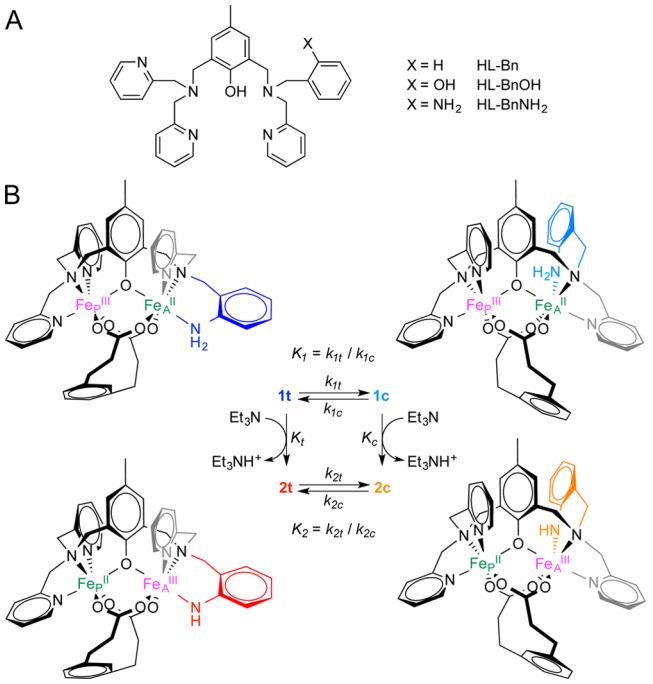

[a]The deprotonation of complexes **1t** and **1c** by NEt$_3$ is associated with the acid constants K_t and K_c, respectively. A schematic view of the four complexes is proposed, with a unified color code, i.e., aniline in blue, anilide in red, Fe^{II} in green, and Fe^{III} in magenta, used throughout all of the figures.

the same isomerization process within the two complexes, with the aniline or anilide and pyridine arms exchanging their respective positions cis and trans to the bridging phenoxide. This conclusion is supported in the case of **2** by theoretical calculations. Accordingly, we note **1t**, the initial form of **1** obtained upon dissolution of the solid in acetonitrile, and **1c**, the form of **1** after transformation. Similarly, we note **2t**, the major deprotonated form obtained after equilibration, and **2c**, the other one. The transformations are summarized in Scheme 1B, where Fe$_P$ stands for the Fe ion bonded only to two pyridine rings, while Fe$_A$ stands for the Fe ion coordinated to the aniline or anilide ring and one pyridine, independent of the valence of each ion.

RESULTS AND DISCUSSION

Aniline Complexes. The following section is structured to guide the reader through characterization of species **1t** and **1c**, relying successively on ^{1}H NMR, Mössbauer, and UV−visible absorption spectroscopies. We demonstrate (i) that a single species (**1t**) is present immediately after dissolution of **1** in acetonitrile and (ii) that complex **1t** spontaneously evolves to generate complex **1c** in a 35:65 **1t**/**1c** ratio at completion. Last, the kinetics of this conversion is investigated.

Spontaneous Evolution of Complex 1 and Investigation at Completion. Figure 1 reproduces the low field (from 550 to 130 ppm) and high field (from 0 to −80 ppm) ranges of the ^{1}H NMR spectra recorded either immediately or

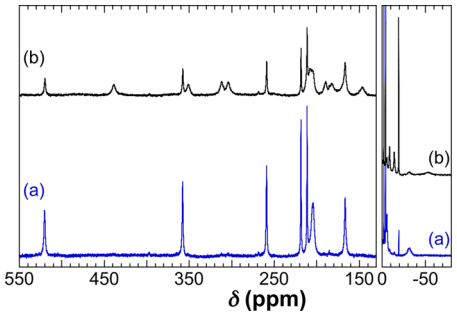

Figure 1. 550−130 and 0 to −80 ppm domains of the ^{1}H NMR spectra recorded at 293 K immediately (trace a, dark-blue line) and 120 min (trace b, black line) after complex **1** was dissolved in CD$_3$CN. A vertical shift was operated on trace b on the right part to evidence the increasing intensity of the −19 ppm signal.

2 h after dissolution of complex **1** in acetonitrile. The full spectra are shown in Figure S1 in the Supporting Information (SI). The starting spectrum (spectrum a) extends from +520 to −35 ppm, as is usual in this series of Fe^{III}Fe^{II} complexes with Fe valences localized on the ^{1}H NMR time scale.[10,11] It is worth noticing that it is similar to that of the complex [(L-Bn)Fe^{III}(μ_2-mpdp)Fe^{II}(NCCH$_3$)]$^{2+}$ (Scheme 1A), indicating that Fe^{III} is in the bis(picolylamine) site.[12] In addition, the number of resonances detected in the low-field window reveals that a single species, further denoted as **1t**, is present. It is thus reasonable to assume that the solution structure of **1t** is identical with the X-ray structure with the aniline ligand coordinated to the Fe^{II} ion in the trans position with respect to the bridging phenoxide.

A total of 2 h after dissolution, spectrum b is detected and remains unchanged with time. Compared to spectrum a, a new set of resonances is present that has grown in at the expense of the peaks of **1t**. This suggests that the species **1t**, solely present immediately after dissolution of complex **1**, spontaneously transforms into a second form, hereafter denoted as **1c**. The spectrum of **1c** extends from +440 to −60 ppm, in agreement with a Fe^{III}Fe^{II} species with localized valences.

Investigation of the temperature dependence of the ^{1}H NMR spectra strongly suggests that **1t** and **1c** interconvert in equilibrium (Figure S2 in the SI). To determine the **1t**/**1c** ratio at completion, the proportion of **1c** was taken as the intensity of the growing peak at −19 ppm and that of **1t** as a third of the combined intensities of the three decreasing resonances at −2, −4, and −5.5 ppm (see Figure S3 in the SI). Figure 2 shows that the proportion of **1c** continuously increases to reach a plateau at ≈0.65. Therefore, when the spontaneous evolution of complex **1** is complete, the resulting solution is a mixture of **1t** and **1c** in a ≈35:65 ratio. The same conclusion was reached by considering other signals for **1c** (at 438, 310, and 304 ppm) and **1t** (at 520 and 258 ppm) (Figure S4 in the SI). A value of 1.8 ± 0.3 is thus obtained for the equilibrium constant K_1.

To investigate the potential changes in the coordination sphere of the Fe sites, Mössbauer spectra were recorded at 80 K and zero field on freshly prepared and equilibrated CH$_3$CN solutions of complex **1** (Figure 3, spectra a and b, respectively). The two spectra were simulated with the same nuclear parameters (Table 1) under the hypothesis that they result from mixtures of two diiron species in different proportions. The resulting nuclear parameters of the two complexes are perfectly consistent with Fe^{III}Fe^{II} species. The parameters of the

dx.doi.org/10.1021/ic501793v | Inorg. Chem. 2014, 53, 10060−10069

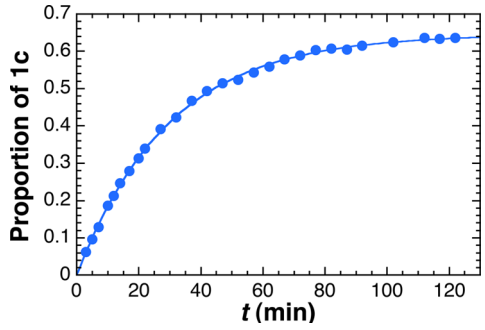

Figure 2. Time dependence of the proportion of form **1c** from ^{1}H NMR spectra recorded at 293 K since dissolution of complex **1** in acetonitrile (blue dots). The solid line corresponds to the best fit according to eq S1a in the SI.

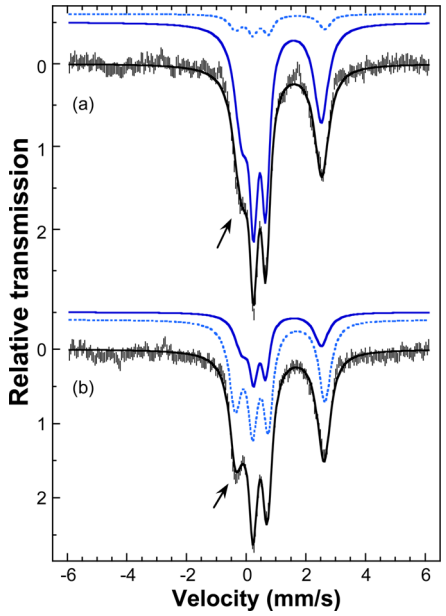

Figure 3. Zero-field Mossbauer spectra scaled to the same area recorded at 80 K (hashed lines) on an acetonitrile solution of complex **1** separated in two cups frozen either briefly (a) or 4 h (b) after dissolution. The arrow indicates the main dissimilarity between the two spectra. The black solid lines correspond to the theoretical spectra calculated according to the parameters listed in Table 1. The contributions of complexes **1t** and **1c** are shown as dark-blue solid and light-blue dotted lines, respectively.

Table 1. Mössbauer Parameters for Complexes 1t, 1c, 2t, and 2c in an Acetonitrile Solution

		δ (mm s^{-1})	ΔE_Q (mm s^{-1})	% in spectrum a[a]	% in spectrum b[a]
1t	Fe^{III}	0.46(1)	0.41(2)	89	33
	Fe^{II}	1.19(1)	2.67(2)		
1c	Fe^{III}	0.49(1)	0.52(2)	11	67
	Fe^{II}	1.14(1)	3.00(2)		
2t	Fe^{III}	0.56(1)	1.75(2)	45	77
	Fe^{II}	1.15(1)	2.55(2)		
2c	Fe^{III}	0.39(1)	0.80(2)	55	23
	Fe^{II}	1.16(1)	3.15(2)		

[a]Labels of Mössbauer spectra refer to Figure 3 for complexes **1t** and **1c** and to Figure 6 for complexes **2t** and **2c**.

major species present in the initial solution are close to those determined for **1** in the solid state (Fe_p^{III}, δ = 0.46(1) mm s^{-1}, ΔE_Q = 0.33(2) mm s^{-1}; Fe_A^{II}, δ = 1.13(1) mm s^{-1}, ΔE_Q = 2.62(2) mm s^{-1}; see Figure S7 in the SI), strongly suggesting that **1t** is the single form of complex **1** present immediately after dissolution. Interestingly, the composition of the equilibrated acetonitrile solution deduced from these simulations (**1t**:**1c** = 33:67) matches perfectly that obtained from the ^{1}H NMR experiment.

Mössbauer spectroscopy thus confirms the presence of **1t** as the major species immediately after dissolution and of two mixed-valent species in a ≈35:65 ratio in the equilibrated acetonitrile solution of **1**. Moreover, the nuclear parameters of the two species are globally highly similar, suggesting a small structural difference between **1t** and **1c**. This dissimilarity is more important for the Fe^{II} sites than for their Fe^{III} counterparts: this may suggest that the difference between **1t** and **1c** is located on the Fe^{II} site. This is indeed confirmed by UV−visible absorption spectroscopy.

Figure 4 reproduces the evolution over 2.5 h of the UV−visible spectra recorded at 295 K after dissolution of complex **1**

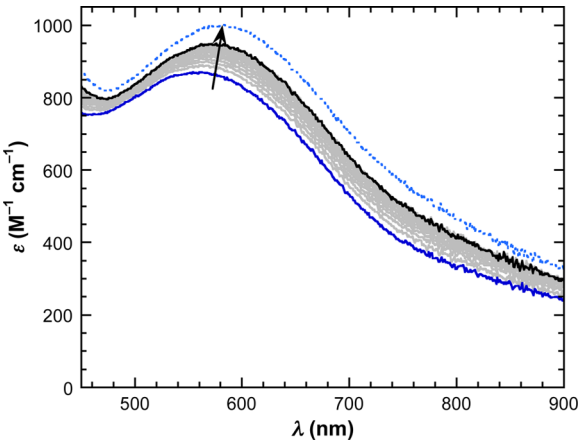

Figure 4. Evolution at 295 K of the UV−visible absorption spectrum of complex **1** upon dissolution in CH_3CN. The vertical axis is scaled to the absorption of the diiron species in a molar concentration according to the Beer−Lambert law, which is equivalent to a molar extinction coefficient. A selection of 16 spectra recorded every 10 min during 2.5 h are reproduced (the first and last spectra are shown as dark-blue and black solid lines, respectively). The calculated signature of **1c** is shown as the light-blue dotted line (see eq S1d in the SI). The arrow is a guide to indicate the increase in the intensity and bathochromic shift.

in acetonitrile. We may hypothesize from the previous results that the spectrum of **1t** coincides with the first recorded spectrum. The signature of **1c** can thus be deduced assuming a ≈35:65 **1t**/**1c** ratio at completion (see eq S1d in the SI). It is reproduced in Figure 4 as the light-blue dotted line. The signatures of **1t** and **1c** are quite similar (**1t**, λ_{max} = 564 nm, ε_{564} = 875 M^{-1} cm^{-1}; **1c**, λ_{max} = 583 nm, ε_{583} = 1000 M^{-1} cm^{-1}). Because the observed absorption is associated with the phenoxide-to-Fe^{III} charge-transfer transition,[11] such small variations suggest that the transformation occurs on the Fe^{II} site. This is fully consistent with the Mössbauer studies.

Kinetics of the 1t ⇆ 1c Conversion. Spectra were recorded regularly during 2 h in ^{1}H NMR and during 2.5 h in UV−visible absorption spectroscopy, thus allowing determination of the rate constants (see eq S1a,b in the SI). The fit of the NMR data leads to $k_{1t} + k_{1c}$ = 0.03(1) min^{-1}, whereas that

dx.doi.org/10.1021/ic501793v | Inorg. Chem. 2014, 53, 10060−10069

from UV−visible gives $k_{1t} + k_{1c} = 0.02(1)$ min^{-1} (see Figures 2 and S8 in the SI, respectively). Satisfyingly, the two sets of data give similar results. Owing to the relationship between K_1, k_{1t}, and k_{1c}, one gets from the NMR fit $k_{1t} = 0.02(1)$ min^{-1} and $k_{1c} = 0.01(1)$ min^{-1}.

Anilide Complexes. To gain further insight into the chemical nature of complex **1c**, we took advantage of the capability of the aminophenyl ligand to be deprotonated by nitrogenous bases. We will show in this section that (i) the deprotonation of the two forms **1t** and **1c** leads to two different forms of complex **2**, thereafter denoted as **2t** and **2c**, (ii) these forms also interconvert, and the **2t**:**2c** ratio is close to 85:15 at completion, and (iii) the rate of the **2t** ⇆ **2c** interconversion is 10 times faster than that between **1t** and **1c**. Last, titration experiments show that **1t** and **1c** have significantly different acid strengths.

Formation of 2t and 2c and Investigations at Completion. Figure 5 shows the absorption spectra recorded

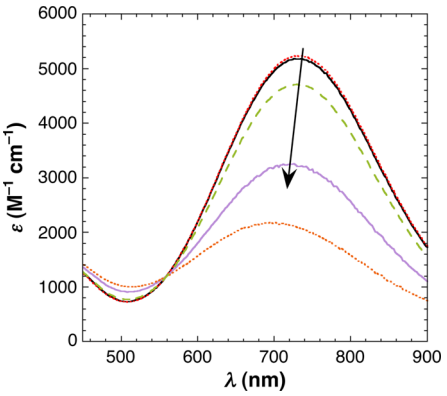

Figure 5. UV−visible absorption spectra recorded at 295 K immediately after the addition of 1.5 equiv of NEt_3 on two solutions of **1t** and **1c** complexes (solid traces). The base was added at 50 s (black) or 120 min (mauve) after dissolution of complex **1** in CH_3CN. The arrow is a guide to visualize the decreasing intensity and the hypsochromic shift upon increasing the amount of **1c** from 2% to 65% in the **1t**/**1c** mixtures when NEt_3 is added. The dotted red and dotted orange lines correspond to the spectra of complexes **2t** and **2c**, respectively, that can be deduced from this series (see eq S2b in the SI). The dashed light-green line is the common spectrum recorded 18 min after the addition of NEt_3, whatever the **1t**/**1c** ratio in the starting solution.

at 295 K immediately after the addition of 1.5 equiv of NEt_3 to two different CH_3CN **1t**/**1c** mixtures. In a first experiment, the base is added 50 s after the dissolution of complex **1** (see the black solid line). The short time elapsed between dissolution and the addition of base implies that the form **1t** is quasi-exclusively present (see above). The addition of base leads to an intense absorption detected at 732 nm ($\varepsilon_{732} = 5190$ M^{-1} cm^{-1}). In a second experiment, another aliquot of the same solution of **1** was allowed to evolve for 120 min before the addition of NEt_3 (see the mauve solid line). This 2 h evolution allows completion of the **1t** ⇆ **1c** equilibrium. Consequently, NEt_3 is added on a 35:65 **1t**/**1c** mixture. An intense but weaker absorption is then detected at 724 nm ($\varepsilon_{724} = 3260$ M^{-1} cm^{-1}). We knew from the previous study that deprotonation is a fast process.[9] The difference between the spectra obtained from these two solutions thus suggests that the addition of base leads to the generation of two different forms of the deprotonated complex **2**, **2t** and **2c** originating from **1t** and **1c**, respectively. This is indeed confirmed by the spectra recorded when base is added on mixtures of **1t** and **1c** with different **1t**/**1c** ratios (see Figure S11 in the SI). Assuming that **2t** and **2c** are present in the proportion of the original **1t**/**1c** ratios allows one to confirm the rate constants of the **1t** ⇆ **1c** conversion and to deduce the signatures of the two forms **2t** and **2c** (see Figure S12 and eq S2b in the SI). They are shown as dotted red and dotted orange lines in Figure 5, respectively. They differ slightly in the wavelength of the absorption maximum, 730 nm for **2t** versus 700 nm for **2c**, and mostly by the associated value of the molar extinction coefficient, $\varepsilon_{730} = 5240$ M^{-1} cm^{-1} for **2t** versus $\varepsilon_{700} = 2175$ M^{-1} cm^{-1} for **2c**. Such an intense absorption is reminiscent of the anilide-to-Fe^{III} charge-transfer transition previously observed in a mononuclear iron(III) complex.[13] Such large variations in the intensity strongly suggest that the change between the forms **2t** and **2c** occurs on the Fe^{III} center.

As indicated below and detailed in the SI, the evolution of the absorption spectra shown in Figure 5 stopped after ≈14 min, indicating completion of the evolution. Figure 5 also reproduces the spectrum recorded 18 min after the addition of 1.5 equiv of NEt_3 (see the dashed light-green trace). The same spectrum is obtained whatever the moment the base is added after dissolution of complex **1**. It is worth noticing that all of these spectra, including those of **2t** and **2c**, present the same absorption at 559 nm, evidencing an isosbestic point. We thus hypothesized that the **2t** and **2c** starting mixtures spontaneously evolve by interconversion between the two species (see Scheme 1B). Indeed, the spectrum at completion can be satisfyingly reproduced by a linear combination of the **2t** and **2c** spectra. The best agreement is obtained for a 83:17 **2t**/**2c** ratio, leading to the equilibrium constant $K_2 = 0.20(5)$.

These UV−visible studies suggest that the forms **2t** and **2c** differ by the coordination on the Fe^{III} site. To confirm this hypothesis, Mössbauer spectra were recorded on an equilibrated solution of complex **1** in order to maximize the proportion of species **2c** immediately after the addition of the base. Figure 6 reproduces the spectra recorded at zero field and 80 K on a 35:65 **1t**/**1c** solution frozen either shortly after the addition of the base (spectrum a) or 10 min after (spectrum b). They clearly evidence a time dependence of the solution composition. These spectra can be well reproduced by assuming the presence of two mixed-valent diiron complexes in different proportions (see Table 1). According to UV−visible studies, species **2t** is the predominant complex at longer time (83:17 **2t**/**2c**). Interestingly, it is the minor species in spectrum a, as expected when starting from a 35:65 **1t**/**1c** mixture. The isomer shift values [**2t**, 0.56(1) and 1.15(1) mm s^{-1}; **2c**, 0.39(1) and 1.16(1) mm s^{-1}] are consistent with mixed-valent Fe^{III}Fe^{II} species with high-spin ions. The 0.39 mm s^{-1} isomer shift determined for the Fe^{III} center of **2c** is smaller than the 0.45−0.55 mm s^{-1} values usually observed for high-spin Fe^{III} ions.[14] However, values between 0.40 and 0.44 mm s^{-1} have already been reported for high-spin Fe^{III} ions in a quite similar environment.[12,15−17] It must be underlined that the ΔE_Q values of the Fe^{III} ion are very large in both complexes and even larger in **2t** than in **2c** [1.75(2) vs 0.80(2) mm s^{-1}, respectively]. This large variation sustains a change on the ferric center between the two forms **2t** and **2c**.

To gain more information on the nature of the two forms **2t** and **2c**, ^{1}H NMR spectra were recorded. To optimize the quantity of **2c**, 1.5 equiv of NEt_3 was added on a 35:65 **1t**/**1c** solution. The progressive disappearance of several resonances is detected (see Figures S13 and S14 in the SI). This is in

dx.doi.org/10.1021/ic501793v | Inorg. Chem. 2014, 53, 10060−10069

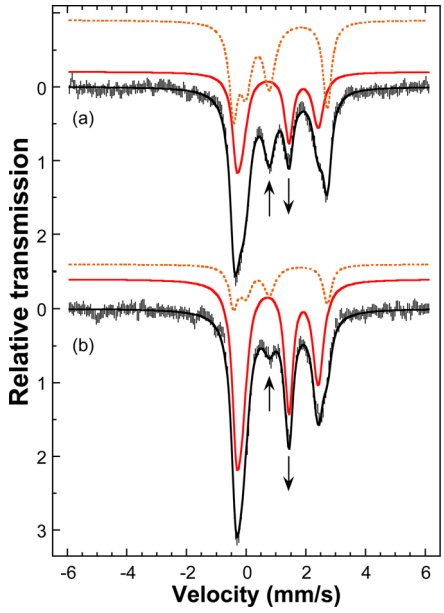

Figure 6. Zero-field Mössbauer spectra recorded at 80 K after the addition of 1.5 equiv of NEt_3 on a CH_3CN 35:65 **1t**/**1c** solution (hashed marks) separated in different cups that were frozen shortly (a) or 10 min (b) after the addition of the base. The arrows evidence the changes in the relative line intensities. The black solid lines correspond to the theoretical spectra calculated according to the parameters listed in Table 1. Contributions of complexes **2t** and **2c** are shown as solid red and dotted orange lines, respectively.

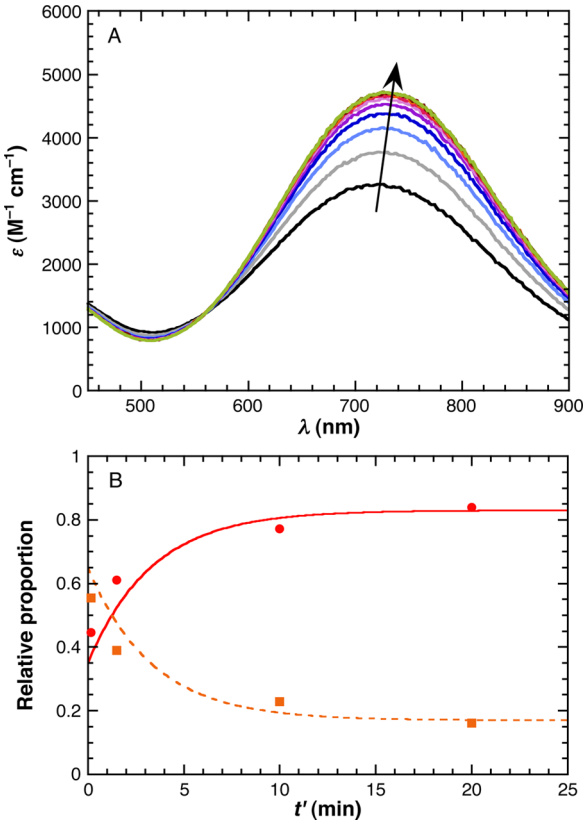

Figure 7. (A) Evolution at 295 K of the UV−visible absorption spectra when 1.5 equiv of NEt_3 are added on a 35:65 **1t**/**1c** solution (colored solid lines). A total of 11 spectra regularly recorded over 16 min are shown. The arrow is a guide to indicate the increase in the intensity and the bathochromic shift. (B) Time dependence of the relative proportions of complexes **2t** (full red circles) and **2c** (full orange squares) as obtained from simulations of Mössbauer spectra (see the caption of Figure S15 in the SI). t' stands for the time since the addition of 1.5 equiv of NEt_3 on a 35:65 **1t**/**1c** solution. The solid red and dotted orange lines correspond respectively to the theoretical distribution of complexes **2t** and **2c** calculated by assuming k_{2t} = 0.05 min^{-1} and k_{2c} = 0.25 min^{-1} as determined from UV−visible absorption experiments.

agreement with the formation of **2t** and **2c**, which further interconvert, leading to the prevalence of **2t** at equilibrium completion, as detected by both UV−visible and Mössbauer spectroscopy. Indeed, the major species in solution at completion is characterized by two signals at −214 and −243 ppm (Figure S13 in the SI). By contrast, the more upfield-shifted resonance of **2c** is detected at −15 ppm.

Kinetics of the 2t ⇆ 2c Conversion. The **2t** ⇆ **2c** conversion was monitored by UV−visible absorption spectroscopy. Spectra were recorded at 295 K over ≈18 min after the addition of 1.5 equiv of NEt_3 on a CH_3CN solution of complex **1**. Seven cuvettes were prepared that differ in the time lag between the dissolution of **1** and the addition of the base. It increases from 50 s to 120 min so that the solution of **1** has evolved from a ≈100:0 to a ≈35:65 **1t**/**1c** composition (see Figures 7A and S9 in the SI). As detailed in the SI, all of these data sets can indeed be fully accounted for upon assuming that the two starting complexes **1t** and **1c** have been converted to **2t** and **2c**, which further interconvert (Scheme 1B). The fits of the time dependence of the ε values at 720 nm lead to $k_{2t} + k_{2c}$ = 0.30(2) min^{-1}, whatever the composition of the starting solution (see Figure S10 in the SI). Keeping in mind that the equilibrium constant K_2 is equal to 0.20(5), calculations of the two rate constants k_{2t} and k_{2c} give 0.05(2) and 0.25(2) min^{-1}, respectively. Accordingly, Figure 7B reproduces the theoretical time dependence of the proportions of **2t** and **2c** when NEt_3 is added on a 35:65 **1t**/**1c** solution (solid red and dotted orange lines, respectively). It is worth noticing that the four Mössbauer spectra recorded after the addition of a base on a similar 35:65 **1t**/**1c** solution lead to relative proportions of **2t** and **2c** complexes, in full agreement with the kinetics deduced from UV−visible investigations (see full dots in Figures 7B and S15 in the SI).

Acid Strengths of 1t and 1c. The two chromophores present different ratios in the **t** versus **c** forms: 35:65 for the acidic form **1** and 83:17 for the basic form **2**. This evidences different acid strengths for **1t** and **1c**. Taking into account the time required to reach equilibrium for **2t**/**2c** mixtures, a titration of the 35:65 **1t**/**1c** solution was performed. Figure 8 reproduces the spectra recorded at 295 K and 17 min after the addition of up to 4 equiv of NEt_3. Two isosbestic points are observed at 485 and 547 nm, indicating that two chromophores coexist in solution. The inset in Figure 8 shows variation of the molar extinction coefficient at 720 nm as a function of the number of added equivalents of NEt_3. These data can be satisfyingly reproduced by considering deprotonation of the 35:65 **1t**/**1c** chromophore by NEt_3, leading to the 83:17 **2t**/**2c** chromophore in addition to Et_3NH^+. K_{app} = 34(3) is determined for the equilibrium constant associated with this reaction (eq S3a in the SI).

It can be anticipated that the addition of aliquots of base disrupts both the 35:65 **1t**/**1c** and 83:17 **2t**/**2c** ratios. However, these ratios are recovered within less than 20 min, a relatively short time period in contrast with the large one (2 h) necessary

dx.doi.org/10.1021/ic501793v | Inorg. Chem. 2014, 53, 10060−10069

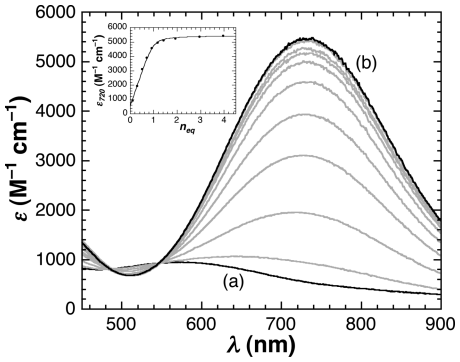

Figure 8. Evolution at 295 K of the UV−visible absorption spectrum of a CH_3CN solution of complexes **1t** and **1c** in a 35:65 ratio upon the addition of 0 (curve a) to 4 equiv (curve b) of NEt_3. The inset reproduces the evolution at 720 nm as a function of the number of added equivalents of NEt_3 (full circles). The black solid line corresponds to the best fit according to eq S3a in the SI.

for complete **1t** ⇆ **1c** reequilibration in the absence of base. As demonstrated in Figure S16 in the SI, the rate of the interconversion between complexes **1t** and **1c** is indeed controlled by that of the conversion between the deprotonated complexes **2t** and **2c** and the fast acid−base equilibria. In other words, **1c** is generated from **1t** through successive reactions **1t** → **2t** → **2c** → **1c**. Moreover, in conjunction with the two other equilibrium constants K_1 and K_2, the acid strengths K_t and K_c of the two aniline complexes **1t** and **1c**, when deprotonated by NEt_3, can be determined (Scheme 1B and eq S3b,c in the SI). One gets K_t = 83(10) and K_c = 9(3), indicating that **1t** is ca. 1 order of magnitude more acidic than **1c**.

Structure of the Aniline and Anilide Complexes. The studies presented above clearly demonstrate that both complexes **1** and **2** exist in acetonitrile solutions under two forms, with **2t** (respectively **2c**) resulting from the deprotonation of complex **1t** (respectively **1c**). Relying on the spectroscopic features, we will discuss here the chemical nature of these forms.

All spectroscopic data are consistent with **1t** retaining in solution the structure determined by crystallography, with the aniline ligand bound to the Fe^{II} ion, therefore denoted as Fe_A^{II}. Two hypotheses can be envisioned for the structure of **1c**: (i) a valence isomer, $[(L\text{-}BnNH_2)Fe_P^{II}(\mu_2\text{-mpdp})Fe_A^{III}]^{2+}$, where the Fe^{II} and Fe^{III} sites are interchanged and (ii) a coordination isomer where the aniline and pyridine have interchanged position, with the pyridine being trans and the aniline cis to the bridging phenoxide.

We believe that hypothesis i is less likely. Indeed, the valence inversion would lead to an Fe^{II} ion in the bis(picolylamine) site, whereas all X-ray structures of $M^{III}M^{II}$ complexes (M = Fe or Mn) of these kinds of ligands with neutral amine donors systematically reveal that this site is occupied by the trivalent metal ion.[10,12,27] Hypothesis ii considers **1c** as a geometrical isomer of **1t**, with the aniline cis and the pyridine trans to the bridging phenoxide (top part of Scheme 1B). This hypothesis is consistent with the observation in Mössbauer spectroscopy that only the Fe^{II} site is modified. Several X-ray structures of similar complexes show that a pyridine can bind in the trans position with respect to the phenoxido bridge,[11,26] thus supporting hypothesis ii. Nevertheless, there is no strong evidence for either of the two hypotheses.

In the **2t** and **2c** complexes, the valences of the two Fe ions are inverted with respect to **1t**, with the Fe^{III} ion being bound to the anilide (therefore denoted as Fe_A^{III}) and the Fe^{II} ion in the bis(picolylamine) site (therefore denoted as Fe_P^{II}). Two particular spectroscopic features of **2t** support that this complex is most probably the trans isomer of the anilide complex. First, its ^1H NMR spectrum (Figure S13 in the SI) presents two characteristic upfield resonances at −214 and −243 ppm. Such negative values are very peculiar and reminiscent of those observed at −100 and −105 ppm on the mixed-valent complex $[(L\text{-}BnO)Fe^{II}(\mu\text{-}O_2P(OPh)_2)_2Fe^{III}]^{2+}$, where HL-BnOH is analogous to HL-$BnNH_2$ with a 2-hydroxyphenyl group in place of the 2-aminophenyl arm (see Scheme 1A).[11] They have been respectively attributed to the para and ortho protons of the terminal phenoxido ring that is coordinated to the Fe^{III} ion in the trans position with respect to the bridging phenoxide. Second, the Fe^{III} ion exhibits an unusually large Mössbauer quadrupole splitting ΔE_Q = 1.75(2) mm s^{-1}. In general, values lying between 0.30 and 0.55 mm s^{-1} are observed for ferric ions in similar N_3O_3 environments with neutral nitrogenous ligands.[12,21,26] In contrast, values higher that 0.95 mm s^{-1} have been previously observed for Fe^{III} sites in similar systems exclusively when an anionic ligand is coordinated trans to the phenoxido bridge, as summarized in Scheme 2 (part c), and are reminiscent of those of μ-oxodiferric entities.[28]

Scheme 2. ΔE_Q Values Determined for Relevant Ferrous and Ferric Sites within Dinuclear Complexes[a]

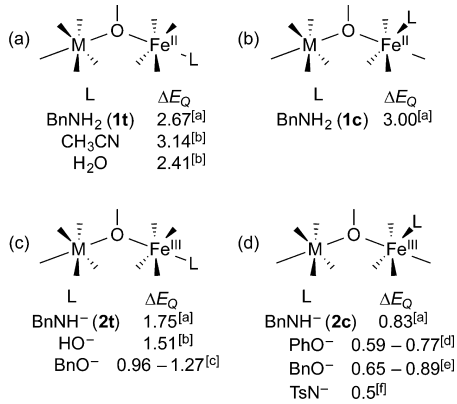

[a]Classification is made to compare to complexes **1t** (part a), **1c** (part b), **2t** (part c), and **2c** (part d). Details on the complexes are given in Table S1 in the SI. [a] This work. [b] See ref 12. [c] See refs 11 and 18−24. [d] See refs 11 and 25. [e] See refs 19 and 23. [f] See ref 26.

The quadrupole splitting of the Fe^{III} site in **2c** is also large [ΔE_Q = 0.80(2) mm s^{-1}] but not as large as that in **2t** [ΔE_Q = 1.75(2) mm s^{-1}]. Similar difference in the ΔE_Q values of the ferric center have been previously observed in the bisferric complexes $[Fe^{III}(BBPPNOL)(\mu\text{-}X)_2Fe^{III}]^+$ [0.89 and 1.27 mm s^{-1} for X = AcO^- [23] and 0.65 and 1.17 mm s^{-1} for X = $(PhO)_2PO_2^-$ [19]], where H_3BBPPNOL stands for *N,N′,N,N′*-bis[(2-hydroxybenzyl)(2-pyridylmethyl)]-2-hydroxy-1,3-propanediamine (see Table S1 in the SI). The X-ray structure of the bis(diphenylphosphato)-bridged complex[19] confirms the presence of one terminal phenoxide ligand in the trans position to the alkoxido bridge, while the other is in the cis position. Because the larger ΔE_Q value indeed originates from the site with trans coordination of the terminal phenoxide, the lower one is attributed to cis coordination. Therefore, the ΔE_Q value

dx.doi.org/10.1021/ic501793v | Inorg. Chem. 2014, 53, 10060−10069

of 0.80(2) mm s^{-1} found for **2c** is consistent with cis coordination of the anilide on the Fe^{III} ion. This assignment is supported by the observation that, for related complexes in this series of ligands, ΔE_Q values in the range of 0.5−0.77 mm s^{-1} are associated with the binding of anionic ligands in the cis position to the bridging phenoxide (Scheme 2, part d).[11,25,26]

To summarize, all spectroscopic features concur to propose that **2t** and **2c** are isomers of the anilide complex, with the anilide occupying respectively the trans or cis position with respect to the bridging phenoxide. Coming back to the aniline complexes, the connection between **1t** and **2t**, on the one hand, and **2c** and **1c**, on the other hand, makes it tempting to assign **1c** as the *cis*-aniline isomer. However, the situation is less clear-cut owing to the similarity of the ligands under consideration, aniline versus pyridine, which are too similar to engender distinct spectroscopic features of the two species. DFT calculations were thus carried out to identify the nature of the aniline and anilide species and gain more insight into their electronic structures in correlation with structural parameters.

DFT Calculations. Our general approach was in all cases to run full geometry optimizations using a generalized gradient approximation (GGA) functional—OPBE, known to give reliable spin-state energetics—followed by single points (SPs) using the hybrid functional B3LYP. The latter SPs were exploited to yield bonding energies, spin densities, and Mössbauer parameters (see below). All procedures are given in the Computational Details section. It should be mentioned that a specific treatment of Fe^{II} Mössbauer parameters has been derived because of the particular electronic structures of these complexes. This is described in the computational part and in the SI. Owing to their more contrasted nature, we started our calculations by considering the anilide complexes **2**.

The starting geometry for **2t** was taken from the X-ray structure of the trans isomer **1t**.[8] After the bridging dicarboxylate ($mpdp^{2-}$) was replaced by two acetate ions and the aniline was deprotonated, we optimized its geometry with Fe valences localized as deduced from spectroscopic analyses, i.e., $Fe_P^{II}Fe_A^{III}$ (the resulting structure is hereafter denoted as 2-TRANS). To study hypothesis ii, trans-to-cis isomerization, we generated **2c** from the structure of **2t** shown in Scheme 1B by inverting the positions of the two branches of the ligand with respect to the Fe−O−Fe plane through rotation of the ligand along the axis passing through the CH_3−C and C−O bonds of the phenoxide. We then optimized its geometry with the same valence localization $Fe_P^{II}Fe_A^{III}$ (the resulting structure is hereafter denoted as 2-CIS). To consider hypothesis i, valence inversion, we optimized the trans isomer with inverted localized Fe valences, i.e., $Fe_P^{III}Fe_A^{II}$ (the resulting structure is hereafter denoted as 2-INV). Whereas calculations of the 2-TRANS and 2-CIS isomers converge to reasonable structures with expected electronic configurations (Table 2), the 2-INV-optimized geometry was found to be at higher energy than both 2-TRANS and 2-CIS conformations by 0.41 eV and converged to a kind of "detrapped" electronic configuration where the spin densities on both Fe ions were similar and reduced to ca. 3 (Table S3 in the SI). All efforts to obtain the 2-INV localized values using special Amsterdam density functional (ADF) procedures to initiate the desired spin polarizations were unsuccessful. This observation supports that **2c** is not the inverted valence trans isomer, which is consistent with the anilide strongly stabilizing the ferric site as expected. Table 2 gathers the main structural parameters of the resulting optimized geometries of the 2-TRANS and 2-CIS conformers,

Table 2. Structural Parameters (Mean Fe−Ligand Bond Length ⟨*d*⟩ and Fe_A−$N_{anilide}$, in Å) for Anilide Complexes (2-CIS and 2-TRANS), As Obtained from OPBE Optimizations Imposing Starting Spin Polarizations (4 for Fe_P and 5 for Fe_A) and Computing the BS State[a]

		2-TRANS	2-CIS
Fe_P	⟨*d*⟩	2.17	2.17
Fe_A	⟨*d*⟩	2.13	2.14
	dN_{anil}	1.96	1.99
	E_b^{B3LYP}	−665.76	−665.75
	ρs Fe_P	−3.74	−3.74
	ρs Fe_A	4.00	4.02

[a]The final bonding energies E_b^{B3LYP} from SPs are given (eV), as well as B3LYP-computed final spin polarizations for both Fe ions.

with bonding energies and final spin densities on both Fe ions to check the actual localization of the valences.

Both isomers are obtained at the same energies, whatever the DFT level (Table S3 in the SI). The mean Fe−ligand distances are consistent with those expected for octahedral high-spin Fe^{II} (Fe_P) and Fe^{III} (Fe_A) ions. The spin densities correspond to the expected ones, with 4.00−4.02 for Fe_A consistent with a "theoretical" value of 5 reduced by polarization donation effects and with 3.74 for Fe_P consistent with a "theoretical" value of 4 reduced also by donation. The spin polarization on the N-donor atom of the anilide ligand is close to 0.4. This indicates a strong donation to the Fe_A^{III} ion, as expected from an anionic N-donor ligand. In contrast, the spin polarization of the oxygen from phenoxide is close to 0 (ca. 0.05), which can be due to, first, the softer character of the N-donor ligand compared to the analogous O-donor one and, second, deactivation of the phenoxide bridging oxygen due to its bonding to the Fe_P ion.

Kohn−Sham orbital diagrams were also examined for both isomers, and the key data are gathered in Table S7 in the SI. Both isomers have very similar orbital diagrams. In particular, these diagrams reveal a strong covalent bonding between Fe_A^{III} and the anilide ligand, best illustrated in Figure S17 in the SI, which represents the singly occupied molecular β-orbital of the 2-TRANS and 2-CIS isomers.

We also calculated the Mössbauer parameters of both 2-CIS and 2-TRANS isomers, for comparison with the experimentally determined parameters of **2t** and **2c**. They are all given in Table 3.

As detailed in the computational section and the SI, a systematic difference is obtained for Fe^{II} in all reference models that we calculated, and as an average, it amounts to ca. 0.25 mm s^{-1}. Adding this value to our calculated ones indeed restores a good estimate. As far as the Fe^{III} ion is concerned, we note that

Table 3. Mössbauer Parameters (δ and ΔE_Q, in mm s^{-1}) Calculated at the B3LYP Level (see the Computational Part) from the Optimized Geometries of the Anilide Isomers 2-CIS or 2-TRANS with $Fe_P^{II}Fe_A^{III}$ Valence, Compared with Experimental Values (T = 80 K) of 2t and 2c[a]

		2-TRANS	2-CIS	2t	2c
δ	Fe_P^{II}	0.92 (1.17)	0.92 (1.17)	1.15	1.16
	Fe_A^{III}	0.58	0.57	0.56	0.39
ΔE_Q	Fe_P^{II}	3.35	3.32	2.55	3.15
	Fe_A^{III}	2.31	1.72	1.75	0.80

[a]In parentheses, δ values for the Fe^{II} ion after correction (see the SI).

dx.doi.org/10.1021/ic501793v | Inorg. Chem. 2014, 53, 10060−10069

the ΔE_Q value of the 2-CIS conformer is significantly smaller than that of the 2-TRANS, as observed experimentally.

In summary, these calculations definitely support that **2c** is the cis isomer of the anilide complex and the similar calculated energies of the two conformers are consistent with their being in equilibrium in solution at room temperature.

Similar calculations were performed for the 1-TRANS, 1-CIS, and 1-INV isomers of **1** analogous to that of **2** (see the SI). They show that the bonding energies of the three aniline isomers are too similar to allow one of them to be eliminated. They are thus consistent with the experimental observations indicating that **1t** and **1c** are spectroscopically very similar and almost isoenergetic.

To summarize the theoretical analyses of the anilide and aniline complexes, our calculations clearly support that **2c** is the *cis*-anilide isomer. By contrast, for the aniline complex **1c**, they did not allow us to discriminate between the cis conformer and the inverted valence isomer. Nevertheless, the strict link demonstrated by UV−visible, Mössbauer, and ^{1}H NMR spectroscopies between **1c** and **2c** (and **1t** and **2t**) supports that they have the same nature and differ only by the protonation state of the aniline/anilide ligand. Overall, the combined experimental evidence and theoretical analyses support that **1c** is the *cis*-aniline conformer.

Isomerization Processes. All of the spectroscopic and computational data accumulated on the solution changes of the aniline and anilide complexes can thus be accounted for by cis/trans isomerization processes (see Scheme 1B). It is interesting to note that **1c** and **2t** are the preponderant isomers once equilibrations are reached. Because pyridine is a stronger ligand than aniline but weaker than anilide, the major isomer presents in both cases the stronger ligand in the trans position to the phenoxido bridge.

Cis/trans isomerization processes within the coordination sphere of a metal have been scarcely reported in the literature. The most investigated ones concern complexes with monodentate ligands such as CO,[29] H^-,[30−32] or Cl^-.[33] In addition, a few reports involved chelating ligands. Using tridentate ligands (L) containing two pyrazole and one phenol groups, Carrano et al. have shown that the homoleptic complexes $[ML_2]$ (M = Co^{II}, Ni^{II}) can exist in the cis and trans forms, with the rate of conversion being strongly dependent on the steric bulk of the ligand.[34] In addition, when the two pyrazole groups are methylated in the 3 and 5 positions, it has been shown that the cis isomer is more stable for the ferrous complex $[FeL_2]$ while the trans isomer is favored for the ferric species $[FeL_2]^+$.[35] A similar dependence has been noted for molybdenum complexes of the same ligands: the molybdenum(VI) complex $[LMoO_2Cl]$ favors the cis isomer, whereas the molybdenum(V) complex $[LMoOCl_2]$ favors the trans isomer.[36] Interestingly, a structure dependence was observed in the O-atom transfer reaction by the molybdenum(VI) complexes, with the trans isomer reacting 20 times faster than its cis counterpart. Cis and trans isomers involving aniline or anilide ligands have only been previously reported in square-planar $[PtL_2]$ complexes, where the chelating ligand L is (*o*-aminophenyl)-diphenylphosphine or its deprotonated form.[37]

Belle et al.[38] have monitored the isomerization of a dicopper complex of a phenol-based tetrapyridyl ligand bearing fluoro substituants by ^{19}F NMR. Although their ligand and the overall structural changes are very similar to ours, pentacoordination of both Cu ions will undoubtedly give rise to isomerization mechanisms different from those involved with the present hexacoordinated Fe ions.

The most common isomerization mechanism of hexacoordinated metal complexes involves a twist of two opposite faces of the octahedron.[39] For the present complexes, an attractive Bailar-type mechanism is the rotation of the N_3 triangular face with respect to the O_3 one if one considers the Fe_A site. Scheme 3 describes the three successive movements that allow the **1t** → **1c** and **2t** → **2c** conversions. The two N_3 and O_3 triangular faces on the Fe_P site also rotate one relative to the other. Note that the chirality of the tertiary amines is preserved. The reverse sequence can be hypothesized to explain the **1c** → **1t** and **2c** → **2t** isomerization processes.

Scheme 3. Proposed Bailar Twist-Type Mechanism for the 1t → 1c and 2t → 2c Isomerization Processes[a]

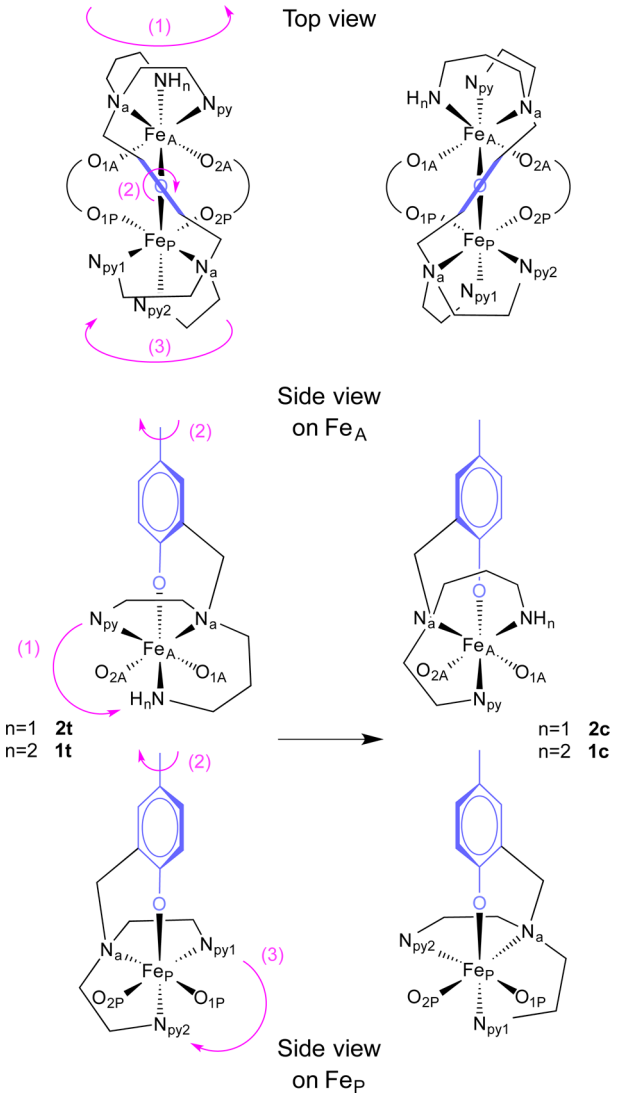

[a]A top view is shown, with a side view along the Fe_A−Fe_P direction focusing on the Fe_A and Fe_P sites, respectively. Arrows indicate the proposed rotations and twist rearrangements.

It follows that the present isomerization of **1** and **2** can be explained by a Bailar mechanism based on the twist of the central phenoxido bridge. Owing to the numerous complexes of this kind, one may wonder why this isomerization process was not observed previously and which specific features made it

dx.doi.org/10.1021/ic501793v | Inorg. Chem. 2014, 53, 10060−10069

possible for **1** and **2**. A total of 21 X-ray structures are reported for diiron complexes that are bridged by two carboxylate groups and a phenoxide substituted in the two ortho positions by $-CH_2-NR_1R_2$ arms. The bridging phenoxide presents the two possible orientations in a 50:50 ratio in all of them except **1**, where a single orientation is observed (Table S2 in the SI). Among the eight complexes having $R_1 \neq R_2$ that could potentially isomerize, **1** is the only one to do it. It is also the only one that possesses a neutral donor engaged in a six-membered metallacycle, with the other complex bearing neutral arms providing five-membered metallacycles only (see Table S2, blue rows, in the SI). This size difference between the two metallacycles may explain why, for neutral chelating groups, isomerization takes place and why the two generated isomers present distinctive spectroscopic features. In the case of **2**, the negatively charged arm is the six-membered metallacycle, with the neutral arm being part of a five-membered metallacycle. No isomerization has been reported for the kind of complexes bearing one negatively charged terminal ligand. This may be traced to a strong preference for the trans isomer, as observed for **2**. We could detect the isomerization of **2** because the trans isomer **2t** is largely favored (**2t**: 83% at equilibrium), and the deprotonation of **1** was initiated in mixtures where the cis isomer **1c** is the major one (**1t**: 35%), thus allowing evolution of the solution composition to be observed.

CONCLUSION

The present study has enlightened the original features related to the intrinsic properties of position isomers of metal complexes. To the best of our knowledge, such a detailed study is unprecedented and was achievable only owing to the very rich and distinctive properties of the systems investigated. As mentioned above, cis/trans isomerization processes within the coordination sphere of a metal have been scarcely reported in the literature. In a number of cases, it was shown that the isomers are not identical in terms of physical properties and reactivities.[32,34−36] The present work indeed substantiates these observations. For the anilides **2t** and **2c**, the two isomers differ in several spectroscopic features: extinction coefficient of the UV−visible absorption, Mössbauer quadrupole splitting, and NMR properties. Indeed, the spectral range of the NMR spectrum of the trans isomer **2t** extends to ca. −250 ppm, with the two resonances corresponding to the *o*- and *p*-anilide protons occurring at −214 and −243 ppm. By contrast, those of the cis isomer **2c** appear in the range 0 to −15 ppm. In addition, a very large quadrupole splitting is observed for **2t** (ΔE_Q = 1.75 mm s^{-1}) with respect to **2c** (ΔE_Q = 0.80 mm s^{-1}). It is likely that these observations reflect the same covalency of the anilide ligand that expands in different directions in the two isomers. It is thus of interest that this interaction manifests itself also in the different acidities of the aniline complex isomers, with **1t** being about 1 order of magnitude more acidic than **1c** (K_t = 83 and K_c = 9). Work is currently underway in our laboratory to further assess the influence of the isomerization of the ligand on the acid/base and redox properties of the complexes.

EXPERIMENTAL SECTION

Materials. Complex **1** was prepared according to the published procedure.[8] Acetonitrile for spectroscopic measurements was distilled under argon over CaH_2 and stored within an inert-atmosphere glovebox. All other reagents were of reagent-grade quality and were used as received.

Physicochemical Studies. ^{1}H NMR spectra were recorded in deuterated acetonitrile on a Bruker AC 200 with a 5 mm indirect detection as described previously.[11] Monitoring of the time dependence of the CD_3CN solution of complex **1** is performed at 293 K on a single NMR tube. A similar procedure was used for the investigation of the ≈35:65 **1t**/**1c** solution with 1.5 equiv of NEt_3. Mass spectra were obtained in the electrospray ionization mode on a LCQ-Finnigan Thermoquest spectrometer equipped with an octupolar analyzer and an ion trap. Electronic absorption spectra were recorded in acetonitrile (0.18 mM solution with 1-cm-optical-length cuvettes) on a Varian Cary 50 spectrometer. A Peltier device was used for temperature control (295 K). The molar extinction coefficient values are calculated according to the Beer−Lambert law, assuming that the concentration is equal to that of the initially introduced complex **1** (optical path length of 1 cm). During the investigation of the behavior of **1t**/**1c** mixtures with NEt_3, complex **1** was dissolved in CH_3CN and the solution divided into separate cuvettes thermostated at 293 K, allowing the addition of base at different times. Mössbauer spectra were recorded on 2 mM solutions of ^{57}Fe fully enriched complexes. The experiments were performed using a horizontal transmission cryostat (Oxford Instruments) and a 50 mCi source of ^{57}Co(Rh) as previously described.[8] All velocity scales and isomer shifts are referred to the metallic iron standard. A unique solution of complex **1** was prepared at 293 K and separated into different cups that were independently frozen at the time *t* indicated in the text. The same procedure was used during the investigation of the time dependence of **2t**/**2c** mixtures (unless otherwise indicated; see the caption of Figure S15 in the SI).

Computational Details. All of our calculations have been performed using the *Amsterdam Density Functional 2010* package.[40,41]

For geometry optimizations, we have chosen the OPBE functional,[42,43] in combination with double- or triple-ζ Slater functions and additional polarization functions (DZP, TZP, or TZ2P sets in ADF) basis sets and small core atomic orbitals. This functional has proven to be very efficient among other GGA functionals for describing spin-state energetics.[44−46] We have carried out some optimizations using the conductor-like screening model COSMO, with a medium dielectric constant due to acetonitrile (ε_r = 37.5). In all cases, the difference in the optimized geometries with gas-phase computations was found to be quite weak. SPs were then performed at the B3LYP level with all electron triple-ζ + one polarization (TZP) basis sets for Fe and double-ζ + one polarization (DZP) for all other atoms, in order to compare the total bonding energies at the B3LYP level, as well as spin densities.

All calculations were run in an unrestricted scheme, by imposing the spin polarization, i.e., the number of major spin (or α) electrons minus the number of minor spin (or β) electrons on each Fe cation, depending on its oxidation state. All Fe^{III} or Fe^{II} ions are taken in a high-spin state. These kinds of binuclear complexes generally exhibit a weak antiferromagnetic coupling; thus, we used the approximation of broken symmetry (BS) states in our approach. This was realized by imposing opposite spin polarizations on each Fe center by the keyword MODIFYSTARTPOTENTIAL. We checked after the self-consistent convergence that the resulting spin densities on Fe ions in the Mulliken population analysis were consistent with the BS state and the expected spin polarizations.

Calculations of the Mössbauer parameters were performed using a previously reported methodology.[47] Indeed, a specific point deserves to be mentioned. The calculated Mössbauer parameters of the Fe^{II} ion differ significantly with the experimental values, with the calculated values of δ being 0.2−0.3 mm s^{-1} lower and those of ΔE_Q ca. 1 mm s^{-1} higher than the experimental values. The difference in ΔE_Q can be attributed to the fact that, in most cases, the measurements were performed at 80 K and ΔE_Q values of high-spin Fe^{II} ions are strongly temperature-dependent owing to the presence of low-lying excited states. That in δ is not fully understood, but calculations of reference literature complexes show the same qualitative and quantitative effect pointing to a ca. 0.25 mm s^{-1} underestimation of δ by the calculated value, as explained in the SI.

dx.doi.org/10.1021/ic501793v | *Inorg. Chem.* 2014, 53, 10060−10069

■ ASSOCIATED CONTENT

Supporting Information

Additional ^{1}H NMR, UV−visible, and Mössbauer spectra, computational details, and the CCDC reference codes for the diiron complexes mentioned in the text. This material is available free of charge via the Internet at http://pubs.acs.org.

■ AUTHOR INFORMATION

Corresponding Authors

*E-mail: genevieve.blondin@cea.fr.
*E-mail: jean-marc.latour@cea.fr.

Notes

The authors declare no competing financial interest.

■ ACKNOWLEDGMENTS

The Agence Nationale de la Recherche (Grants ANR 2010 BLAN 703 and ANR-11-LABX-0003-01) and the Région Rhône-Alpes (Grants CIBLE 07 016335 and CIBLE 08 019180) are gratefully acknowledged for their financial support.

■ REFERENCES

(1) Dickman, M. H. *Acta Crystallogr.* **2000**, *C56*, 58−60.
(2) Song, W.-D.; Yan, J.-B.; Ji, L.-L.; Wang, H. *Acta Crystallogr.* **2008**, *E64*, m549.
(3) Kiskin, M. A.; Aleksandrov, G. G.; Dobrokhotova, Z. V.; Novotortsev, V. M.; Shvedenkov, Y. G.; Eremenko, I. L. *Russ. Chem. Bull., Int. Ed.* **2006**, *55*, 806−820.
(4) Genre, C.; Jeanneau, E.; Bousseksou, A.; Luneau, D.; Borshch, S. A.; Matouzenko, G. S. *Chem.—Eur. J.* **2008**, *14*, 697−705.
(5) Malassa, A.; Görls, H.; Buchholz, A.; Plass, W.; Westerhausen, M. *Z. Anorg. Allg. Chem.* **2006**, *632*, 2355−2362.
(6) Genre, C.; Matouzenko, G. S.; Jeanneau, E.; Luneau, D. *New J. Chem.* **2006**, *30*, 1669−1674.
(7) Carboni, M.; Latour, J.-M. *Coord. Chem. Rev.* **2011**, *255*, 186−202.
(8) Gouré, E.; Thiabaud, G.; Carboni, M.; Gon, N.; Dubourdeaux, P.; Garcia-Serres, R.; Clémancey, M.; Oddou, J.-L.; Robin, A. Y.; Jacquamet, L.; Dubois, L.; Blondin, G.; Latour, J.-M. *Inorg. Chem.* **2011**, *50*, 6408−6410.
(9) Balasubramanian, R.; Blondin, G.; Canales, J. C.; Costentin, C.; Latour, J.-M.; Robert, M.; Savéant, J.-M. *J. Am. Chem. Soc.* **2012**, *134*, 1906−1909.
(10) Kanda, W.; Moneta, W.; Bardet, M.; Bernard, E.; Debaecker, N.; Laugier, J.; Bousseksou, A.; Chardon-Noblat, S.; Latour, J.-M. *Angew. Chem., Int. Ed. Engl.* **1995**, *34*, 588−590.
(11) Lambert, E.; Chabut, B.; Chardon-Noblat, S.; Deronzier, A.; Chottard, G.; Bousseksou, A.; Tuchagues, J.-P.; Laugier, J.; Bardet, M.; Latour, J.-M. *J. Am. Chem. Soc.* **1997**, *119*, 9424−9437.
(12) Chardon-Noblat, S.; Horner, O.; Chabut, B.; Avenier, F.; Debaecker, N.; Jones, P.; Pécaut, J.; Dubois, L.; Jeandey, C.; Oddou, J.-L.; Deronzier, A.; Latour, J.-M. *Inorg. Chem.* **2004**, *43*, 1638−1648.
(13) Schlager, O.; Wieghardt, K.; Nuber, B. *Inorg. Chem.* **1995**, *34*, 6456−6462.
(14) Kim, K.; Lippard, S. J. *J. Am. Chem. Soc.* **1996**, *118*, 4914−4915.
(15) Maeda, Y.; Ishida, A.; Ohba, M.; Sugihara, S.; Hayami, S. *Bull. Chem. Soc. Jpn.* **2002**, *75*, 2441−2448.
(16) Mashuta, M. S.; Webb, R. J.; Oberhausen, K. J.; Richardson, J. F.; Buchanan, R. M.; Hendrickson, D. N. *J. Am. Chem. Soc.* **1989**, *111*, 2745−2746.
(17) Mashuta, M. S.; Webb, R. J.; McCusker, J. K.; Schmitt, E. A.; Oberhausen, K. J.; Richardson, J. F.; Buchanan, R. M.; Hendrickson, D. N. *J. Am. Chem. Soc.* **1992**, *114*, 3815−3827.
(18) Karsten, P.; Neves, A.; Bortoluzzi, A. J.; Lanznaster, M.; Drago, V. *Inorg. Chem.* **2002**, *41*, 4624−4626.
(19) Krebs, B.; Shepers, K.; Bremer, B.; Henkel, G.; Althaus, E.; Müller-Warmuth, W.; Griesar, K.; Haase, W. *Inorg. Chem.* **1994**, *33*, 1907−1914.
(20) Neves, A.; de Brito, M. A.; Drago, V.; Griesar, K.; Haase, W. *Inorg. Chim. Acta* **1995**, *237*, 131−135.
(21) Neves, A.; de Brito, M. A.; Vencato, I.; Drago, V.; Griesar, K.; Haase, W. *Inorg. Chem.* **1996**, *35*, 2360−2368.
(22) Neves, A.; de Brito, M. A.; Vencato, I.; Drago, V.; Griesar, K.; Haase, W.; Mascarenhas, Y. P. *Inorg. Chim. Acta* **1993**, *214*, 5−8.
(23) Neves, A.; Erthal, S. M. D.; Drago, V.; Griesar, K.; Haase, W. *Inorg. Chim. Acta* **1992**, *197*, 121−124.
(24) Nie, H.; Aubin, S. M. J.; Mashuta, M. S.; Wu, C.-C.; Richardson, J. F.; Hendrickson, D. N.; Buchanan, R. M. *Inorg. Chem.* **1995**, *34*, 2382−2388.
(25) Campbell, V. D.; Parsons, E. J.; Pennington, W. T. *Inorg. Chem.* **1993**, *32*, 1773−1778.
(26) Avenier, F.; Gouré, E.; Dubourdeaux, P.; Sénèque, O.; Oddou, J.-L.; Pécaut, J.; Chardon-Noblat, S.; Deronzier, A.; Latour, J.-M. *Angew. Chem., Int. Ed.* **2008**, *47*, 715−717.
(27) Dubois, L.; Xiang, D.-F.; Tan, X.-S.; Pécaut, J.; Jones, P.; Baudron, S.; Le Pape, L.; Latour, J.-M.; Baffert, C.; Chardon-Noblat, S.; Collomb, M.-N.; Deronzier, A. *Inorg. Chem.* **2003**, *42*, 750−760.
(28) Kurtz, D. M., Jr. *Chem. Rev.* **1990**, *90*, 585−606.
(29) Darensbourg, D. J. *Inorg. Chem.* **1979**, *18*, 14−17.
(30) Packett, D. L.; Jensen, C. M.; Cowan, R. L.; Strouse, C. E.; Trogler, W. C. *Inorg. Chem.* **1985**, *24*, 3578−3583.
(31) Rybtchinski, B.; Ben-David, Y.; Milstein, D. *Organometallics* **1997**, *16*, 3786−3793.
(32) Barton, B. E.; Zampella, G.; Justice, A. K.; De Gioia, L.; Rauchfuss, T. B.; Wilson, S. R. *Dalton Trans.* **2010**, *39*, 3011−3019.
(33) Sullivan, B. P.; Meyer, T. J. *Inorg. Chem.* **1982**, *21*, 1037−1040.
(34) Higgs, T. C.; Dean, N. S.; Carrano, C. J. *Inorg. Chem.* **1998**, *37*, 1473−1482.
(35) Higgs, T. C.; Ji, D.; Czernuscewicz, R. S.; Carrano, C. J. *Inorg. Chim. Acta* **1999**, *286*, 80−92.
(36) Hoffman, J. T.; Einwaechter, S.; Chohan, B. S.; Basu, P.; Carrano, C. J. *Inorg. Chem.* **2004**, *43*, 7573−7575.
(37) Cooper, M. K.; Downes, J. M. *Inorg. Chem.* **1978**, *17*, 880−884.
(38) Durot, S.; Hossain, L. H.; Hamman, S.; Jamet, H.; Orio, M.; Gautier-Luneau, I.; Luneau, D.; Philouze, C.; Pierre, J.-L.; Belle, C. *Inorg. Chem.* **2010**, *49*, 7832−7840.
(39) Purcell, K. F.; Kotz, J. C. *Inorganic Chemistry*; W. B. Saunders Co.: Philadelphia, PA, 1977.
(40) te Velde, G.; Bickelhaupt, F. M.; Baerends, E. J.; Fonseca Guerra, C.; van Gisbergen, S. J. A.; Snijders, J. G.; Ziegler, T. *J. Comput. Chem.* **2001**, *22*, 931−967.
(41) *ADF2010*: SCM, Vrije Universiteit: Amsterdam, The Netherlands, 2010; http://www.scm.com.
(42) Hoe, W.-M.; Cohen, A. J.; Handy, N. C. *Chem. Phys. Lett.* **2001**, *341*, 319−328.
(43) Perdew, J. P.; Ernzerhof, M.; Burke, K. *J. Chem. Phys.* **1996**, *105*, 9982−9985.
(44) Derat, E.; Kumar, D.; Neumann, R.; Shaik, S. *Inorg. Chem.* **2006**, *45*, 8655−8663.
(45) Han, W.-G.; Giammona, D. A.; Bashford, D.; Noodleman, L. *Inorg. Chem.* **2010**, *49*, 7266−7281.
(46) Swart, M. *J. Chem. Theory Comput.* **2008**, *4*, 2057−2066.
(47) Gouré, E.; Avenier, F.; Dubourdeaux, P.; Sénèque, O.; Albrieux, F.; Lebrun, C.; Clémancey, M.; Maldivi, P.; Latour, J.-M. *Angew. Chem., Int. Ed.* **2014**, *53*, 1580−1584.